Supporting Information: Interdigitated MgO/Au front selective contacts for enhanced photocatalytic systems based on TiO_2 as light-absorber

Oriol Segura-Blanch*[1,2], Eloi Ros[3], Asier Agrelo-Lestón[2,4,5], Edoardo Maggi[1,2,4], Lorenzo Calvo-Barrio[6,7], Jordi Llorca[2,4], Lluís Soler[2,4], Marcel Placidi[1,2,8], Cristóbal Voz[1,2] Edgardo Saucedo[1,2], Joaquim Puigdollers[1,2]

1. *Universitat Politècnica de Catalunya (UPC), Photovoltaic Lab - Micro and Nano Technologies Group (MNT), Electronic Engineering Department, EEBE, Av Eduard Maristany 10-14, Barcelona 08019, Catalonia, Spain*
2. *Universitat Politècnica de Catalunya (UPC), Barcelona Center in Multiscale Science and Engineering, EEBE, Av Eduard Maristany 10-14, Barcelona 08019, Catalonia, Spain*
3. *Departament de Química Inorgànica, Universitat de Barcelona, Diagonal 645, E-08028, Barcelona, Spain.*
4. *Institute of Energy Technologies and Department of Chemical Engineering, Universitat Politècnica de Catalunya (UPC). Eduard Maristany 16, EEBE, Barcelona 08019, Spain*
5. *Center for Cooperative Research on Alternative Energies (CIC energiGUNE), Basque Research and Technology Alliance (BRTA), Alava Technology Park, Albert Einstein 48, Vitoria-Gasteiz 01510, Spain*
6. *Centres Científics i Tecnològics(CCiTUB), Universitat de Barcelona, Carrer de Lluís Solé i Sabarís 1, 08028 Barcelona,Spain;*
7. *IN2UB, Departament d'Enginyeria Electrònica i Biomèdica, Universitat de Barcelona, Carrer de Martí i Franquès 1, 08028 Barcelona, Spain*
8. *Institut de Recerca en Energia de Catalunya (IREC), Jardins de les Dones de Negre 1, Sant Adrià del Besòs 08930,Catalonia, Spain*

***Corresponding autor:** Oriol Segura-Blanch, oriol.segura.blanch@upc.edu

S1. Experimental section

S1.1. Synthesis of TiO_2 thin films by sol-gel method

All the used chemicals were obtained from Sigma-Aldrich and were used without further purification. Titanium (IV) propoxide was chosen as the sol-gel precursor to prepare TiO_2 thin films. During the preparation, an argon inert atmosphere was created in the mixing beaker to avoid hydrolyzation. Typically, 5 g of precursor were added to a beaker and dissolved in 5 g of absolute ethanol. Later a magnetic stirrer at 100 rpm was used to constantly stir the solution along the whole synthesis. Then, 1 mL of hydrochloric acid (37 %) and 2 mL of water were added dropwise and very slowly to avoid hydrolyzation. Afterwards the solution was agitated during 10 min and diluted in 100 mL of absolute ethanol, followed by 15 min of further stirring. The resulting sol solution was ready to be used and can be preserved for two weeks in the fridge for future uses.

Silicon wafers covered with a thin film of alumina (cSi/Al_2O_x) deposited by Atomic Layer Deposition were used as substrates for the preparation of TiO_2 thin films. Those wafers were cut into squares of 2 cm × 2 cm. The alumina layer was used to electrically insulate the silicon from the TiO_2 and increase the hydrophilicity of the substrate to ensure a good sol impregnation of the surface. Three drops of the sol solution were drop casted over the substrates, which were dried at room temperature for 24 hours. Finally, the samples were calcined at 500 ºC under air atmosphere for four hours (at 5 ºC/min), for the purpose of obtaining anatase films. Since this calcination treatment resulted in cracked TiO_2 thin films, each sample was fabricated stacking 3 layers of TiO_2 to fill the initially generated cracks and effectively cover all the substrate surface. The resulting film weighted around 2-3 mg and had a thickness of ca. 1.5± 0.3 µm.

S1.2. Fabrication of Interdigitated front contacts

Magnesium layers were deposited by vacuum evaporation in a bell jar inside a Leybolds Systems, UNIVEX 350G glovebox system. A vacuum of 10^{-5} mbar was achieved in the bell jar using a mechanical pump and a Leybolds Systems, Turbovac TMP 600C. Magnesium pellets were heated up to evaporation temperature using an Alcatel, HI2000 power supply. When the vacuum conditions were matched, we started heating up the Mg pellets until a stable deposition rate of 0.3-1 A/s was achieved (measured with a calibrated quartz crystal). As soon as the deposition rate stabilizes, we start the deposition aiming to deposit a magnesium layer of 10 nm. Microscope slides, aluminum foil, 0.3 mm Nylon wire and Kapton tape were used to draw the studied patterns over the TiO_2. Once the deposition is completed the samples are stored in the nitrogen inert atmosphere of the glovebox until the gold nanoparticles are deposited or the photocatalyst tested. This is done to avoid uncontrolled oxidation of the Mg.

Au nanoparticles were prepared by drop casting 150 µL of 0.1125 M $HAuCl_4$ over the sample surface. The amount of gold corresponds to a 1:100 ratio in weight between the gold and titanium dioxide. The drop casted samples were dried for 30 min at 50 ºC and then annealed at 300 ºC (at 5 ºC/min) for one hour under air atmosphere to form and anchor the Au nanoparticles on the surface of the sample obtaining the samples shown in Figure 1c.

S1.3. Characterization of the samples

Surface scanning electron microscopy (SEM) images was performed on a Zeiss Neon40 Crossbeam Station instrument at 5.0 kV equipped with a field emission source and an energy-dispersive X-ray spectroscopy (EDXS) tool (INCAPentaFETx3 detector, 30mm^2, ATW2 window) for micro-elemental analysis. The free software Fiji was used to measure the Au particle size and the MgO_x area distribution of the samples. The cross-section structure of the samples was observed by high-angle annular dark-field imaging (HAADS) in a scanning transmission electron microscope (STEM) FEI Titan (60-300 kV) equipped with a high resolution energy-dispersive X-ray spectroscopy (HR-EDXS). The Raman spectra of the anatase film was obtained using a Renishaw's inVia Qontor Raman microscope with two monochromatic light sources: visible laser at 532 nm with a nominal 100 mW output power and infrared laser at 785 nm with a nominal 300 mW output power.

XPS experiments were performed in a PHI 5500 Multitechnique System (from Physical Electronics) with a monochromatic X-ray source (Aluminium Kα line of 1486.6 eV energy and 350 W), placed perpendicular to the analyzer axis and calibrated using the 3d5/2 line of Ag with a full width at half maximum (FWHM) of 0.8 eV. The analyzed area was a circle of 0.8 mm diameter, and the selected resolution for the spectra was 187.5 eV of Pass Energy and 0.8 eV/step for the general spectra and 23.5 eV of Pass Energy and 0.1 eV/step for the spectra of the different elements in the depth profile spectra. All Measurements were made in an ultra-high vacuum (UHV) chamber pressure between 5×10^{-9} and 2×10^{-8} torr.

Time-resolved photoluminescence (TRPL) measurements were performed using an Edinburgh Instruments FS5 spectrofluorometer equipped with an EPL-375 picosecond pulsed diode laser (Edinburgh Instruments) as the excitation source. Photoluminescence decays were recorded at an emission wavelength of 550 nm with a spectral bandwidth of 5 nm. Decay traces were acquired until a peak count of 5000 was reached to ensure sufficient signal-to-noise ratio for reliable fitting. The resulting decay curves were fitted with a bi-exponential decay model using the FluoFit software (PicoQuant), described by:

Equation S1

$$I(t) = A + B_1 e^{-t/\tau_1} + B_2 e^{-t/\tau_2}$$

where B_1 and B_2 are the amplitudes, τ_1 and τ_2 are the characteristic decay times, and A accounts for the background signal. All fits were optimised to yield a reduced chi-squared value of $\chi^2 < 1.2$, confirming the goodness of fit and the validity of the bi-exponential model for all samples.

To provide a representative parameter for comparison, the intensity-weighted average lifetime (τ_avg) was calculated from the fitted parameters according to:

Equation S2

$$\tau_{avg} = \frac{B_1\tau_1^2 + B_2\tau_2^2}{B_1\tau_1 + B_2\tau_2}$$

which reflects the average residence time of photoexcited carriers within the emissive states of the system[1].

S1.4. Hydrogen production measurement

All photocatalytic experiments were carried out under dynamic conditions in a glass tube reactor with an inner diameter of 40 mm, and a height of 145 mm, as described elsewhere[2]. The samples were placed right in the middle of the reactor such that the gaseous reactants would enter through the lower part of the reactor, and the gaseous products would leave from the upper part towards the gas chromatograph. The sample was positioned such that the selective contacts were always facing downwards (illuminated side) and silicon substrate free surface upwards (dark side).

A Dreschel bottle containing a mixture of liquid water and ethanol (9:1 molar) was used to obtain a gaseous flow of reactants. Argon gas was circulated through the Dreschel bottle at room temperature with a constant flow of 20 mL/min dragging ethanol and water molecules in gaseous state towards the reactor.

The light source was placed at the bottom of the reactor facing upwards towards the light-absorber layer of the sample. The light sourced consisted in a Solar Simulator equipped with a Newport 66142 Mercury-Xenon arc lamp (Ushio UXM-52MD) working at 500W (see Figure S1 in the supplementary information). The emitted light passed through a water cooled 6117 Newport Liquid filter (water filter simulating the 1.5AM atmosphere thickness) and 77776 Newport Focusing Assembly that focused the light beam into a single branch optic fiber that introduces the light into the reactor. This set up resulted in an irradiance in the UV-A range (absorption range of TiO_2) of 72 mW/cm^2 over the sample surface. The light irradiance was measured with a UV-A radiation monitor from Solar Light Co.

Gaseous products were monitored on-line every 4 min with a gas chromatograph (Micro-GC Agilent 490) employing three columns: Stabilwax, MS 5 Å and Plot U. Calibration curves were obtained in the concentration range of each product using standard gas mixtures provided by certified mass flow controllers (Bronkhorst) and following standard procedures. Only major productions of hydrogen and acetaldehyde were observed in our reactor showing that the dominant reaction was the ethanol dehydrogenation ($CH_3CH_2OH \rightarrow CH_3CHO + H_2$). However, hydrogen and acetaldehyde were not detected in a 1:1 ratio because part of the photoproduced hydrogen underwent recombination with residual oxygen contained in the photoreactor, altering the results of samples that achieved low hydrogen production rates. For high production rates the acetaldehyde condensed in the liquid membrane filter before entering the gas chromatography instrument to avoid damage of columns.

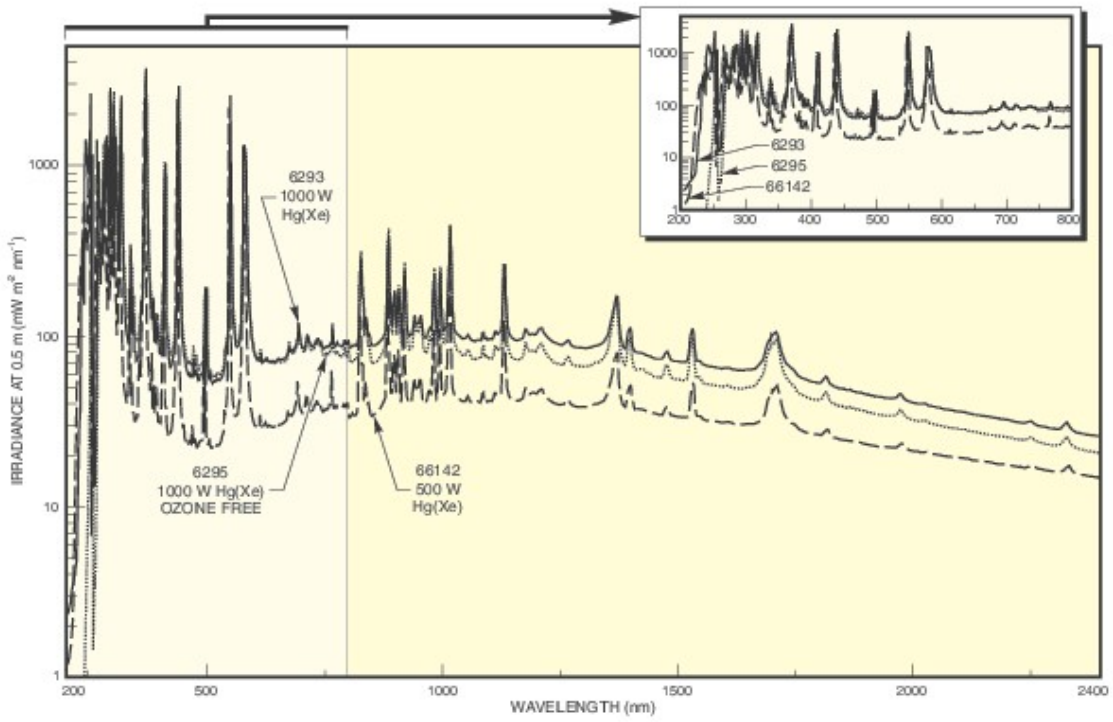

Figure S1. Solar Simulator Lamp Spectra, Newport 66142 Arc Lamp (Ushio UXM-502MD).

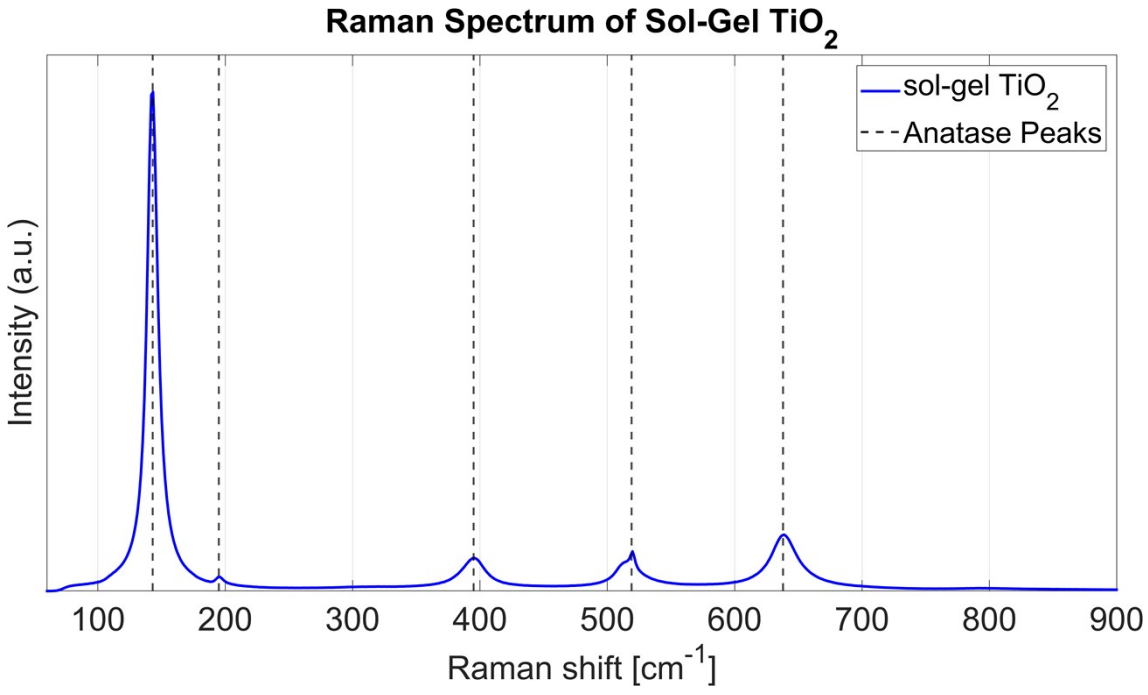

Figure S2. Raman spectra obtained with a green laser excitation for the sol-gel TiO_2 layer deposited on the c-Si/AlO_x substrate.

Table S1. Schematic 3D models of the investigated samples, including sample codes, structural descriptions, and the geometric parameters defining the ETL configuration in each case.

Sketch	Code	Description	Mg Coverage [%]	Mg perimeter [mm]	Geometric factor [η]
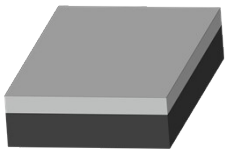	Bare TiO_2	Just the titanium dioxide layer over the silicon/alumina substrate	-	-	-
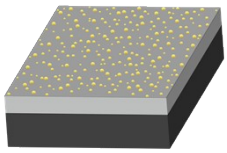	T-Au	Just the titanium dioxide layer over the silicon/alumina substrate with Au NPs on top	-	-	-
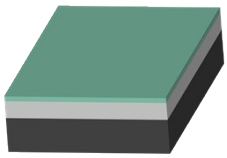	T-Mg1	Titanium dioxide is **totally covered by Mg**	~100	~8	~0.1
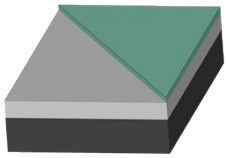	T-Mg2	Titanium dioxide is **half covered by Mg**	~50	~28.3	~0.7
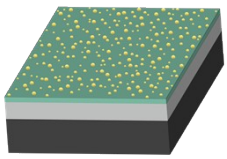	T-Mg1-Au	Titanium dioxide is **totally covered by Mg** and then the Au NPs are deposited	98.6	8.6	0.1
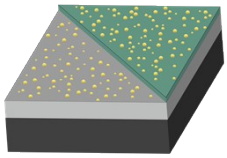	T-Mg2-Au	Titanium dioxide is **half covered by Mg** and then the Au NPs are deposited	50.7	27.6	0.7
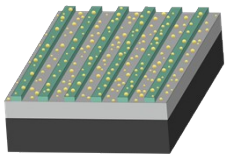	T-Mg3-Au	Titanium dioxide covered **by 6 thick stripes by Mg** and then the Au NPs are deposited	24.3	198.2	10.7
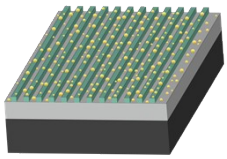	T-Mg4-Au	Titanium dioxide of **25 thin stripes covered by Mg** and then the Au NPs are deposited	53.2	991.4	22.8

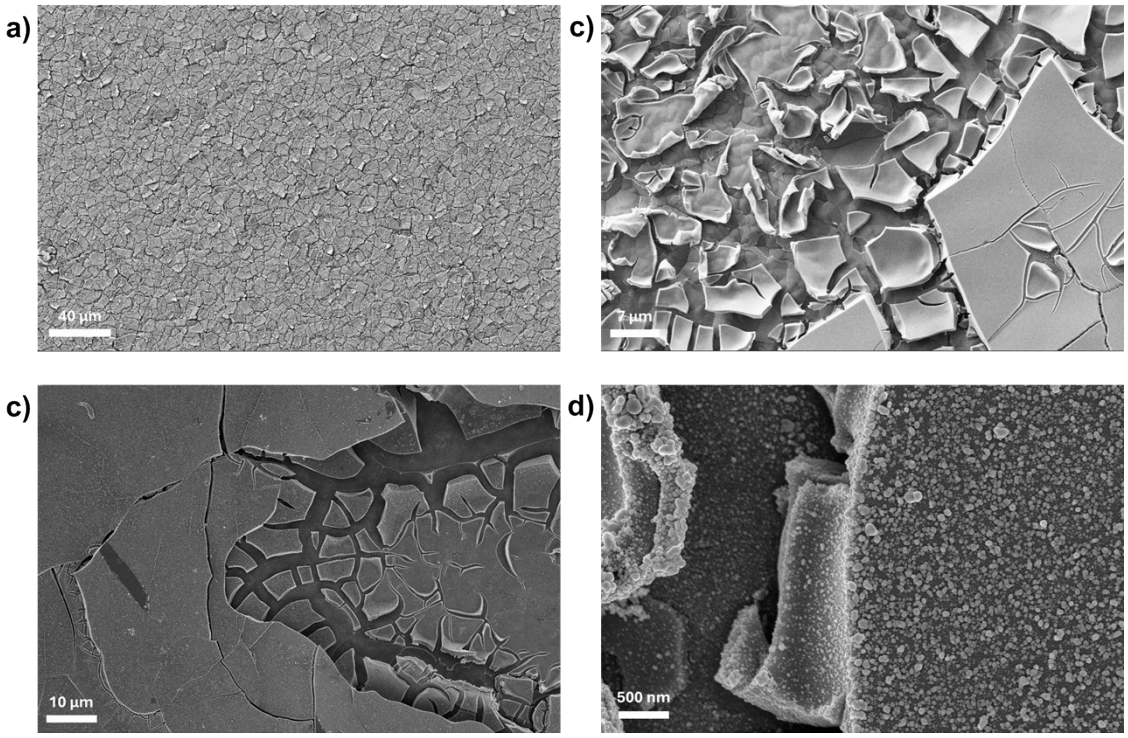

Figure S3 a) Low-magnification image of the bare TiO_2 surface. b) Higher-magnification image of the bare TiO_2 surface. c) Low-magnification image of the T-Mg0-Au sample. d) Higher-magnification image of the T-Mg0-Au sample.

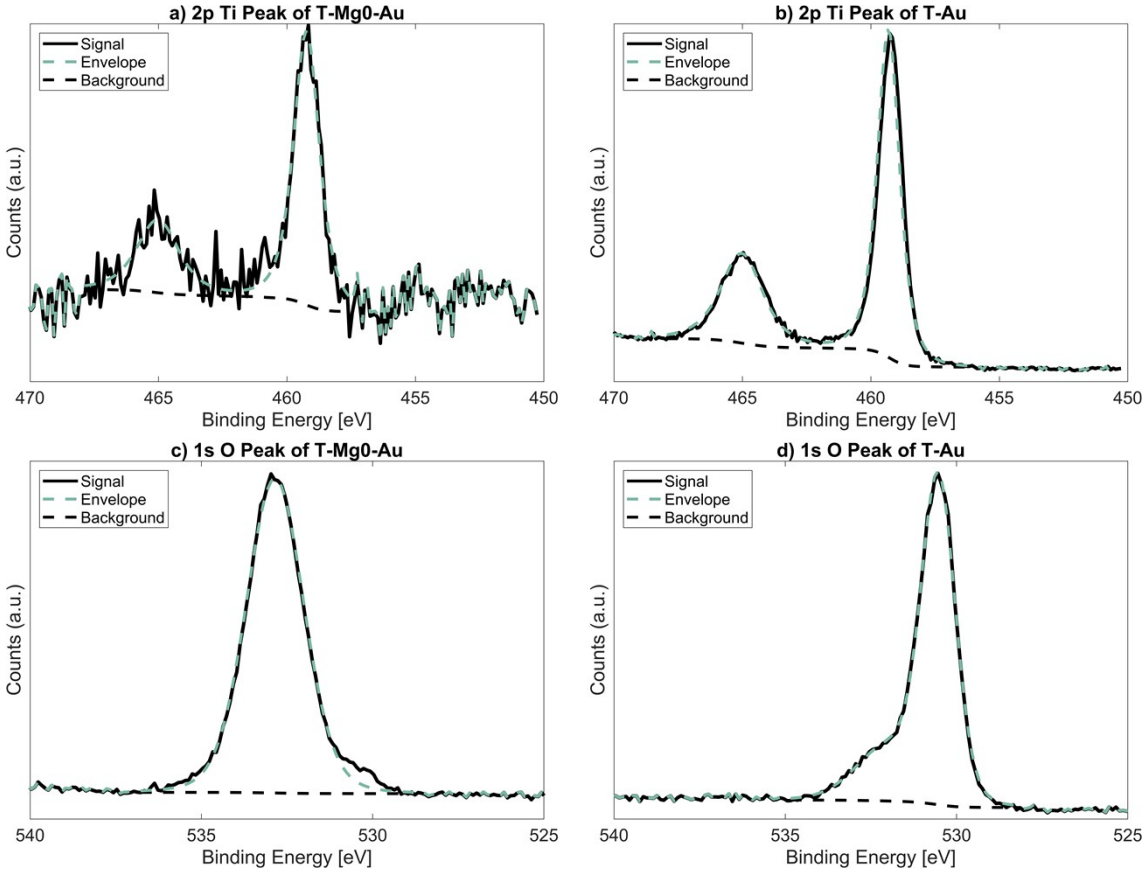

Figure S4 a) Ti 2p XPS peak of the T-Mg0-Au sample. b) Ti 2p XPS peak of the T-Au sample. c) O 1s XPS peak of the T-Mg0-Au sample. c) O 1s XPS peak of the T-Au sample.

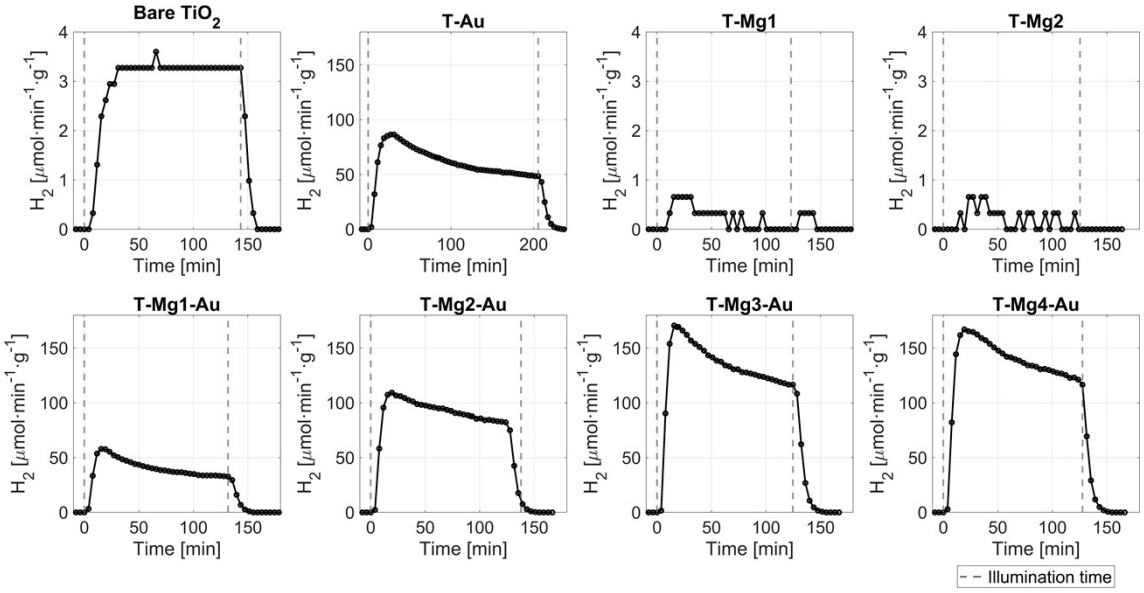

Figure S5. Rate production profiles of hydrogen for the different samples under study.

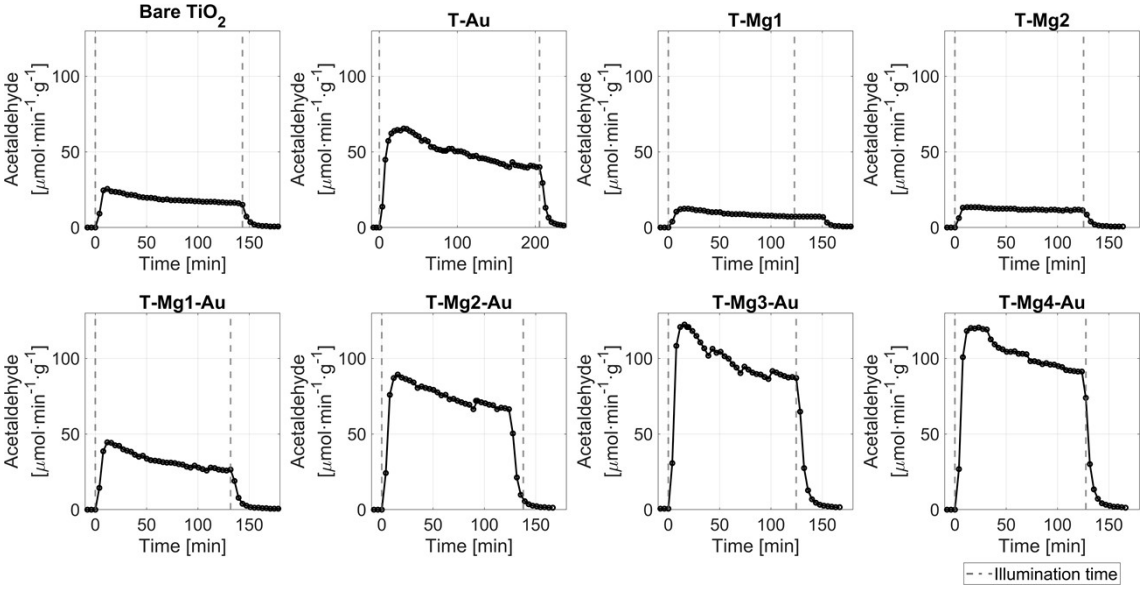

Figure S6. Rate production profiles of acetaldehyde for the different samples under study.

Table S2. Table summarizing the geometric parameters of the ETL patterns for all samples, the amount of hydrogen produced during the first two hours, the mean acetaldehyde production rate over that period, and the corresponding peak acetaldehyde generation rate.

Sample	Mg Coverage [%]	Mg perimeter [mm]	Geometric factor [η]	Acetaldehyde Generated during 2 h [mmol·g^{-1}]	Mean Acetaldehyde Generation Rate [μmol·min^{-1}·g^{-1}]	Maximum Acetaldehyde Generation Rate [μmol·min^{-1}·g^{-1}]
Bare TiO2	-	-	-	2.3	19.0	25.5
T-Au	-	-	-	6.4	53.5	65.5
T-Mg1	~100	~8	~0.1	1.1	9.1	12.4
T-Mg2	~50	~28.3	~0.7	1.4	11.9	13.4
T-Mg1-Au	98.6	8.6	0.1	3.9	32.3	44.5
T-Mg2-Au	50.7	27.6	0.7	8.8	73.0	89.4
T-Mg3-Au	24.3	198.2	10.7	11.6	96.0	122.4
T-Mg4-Au	53.2	991.4	22.8	12.0	99.8	120.5

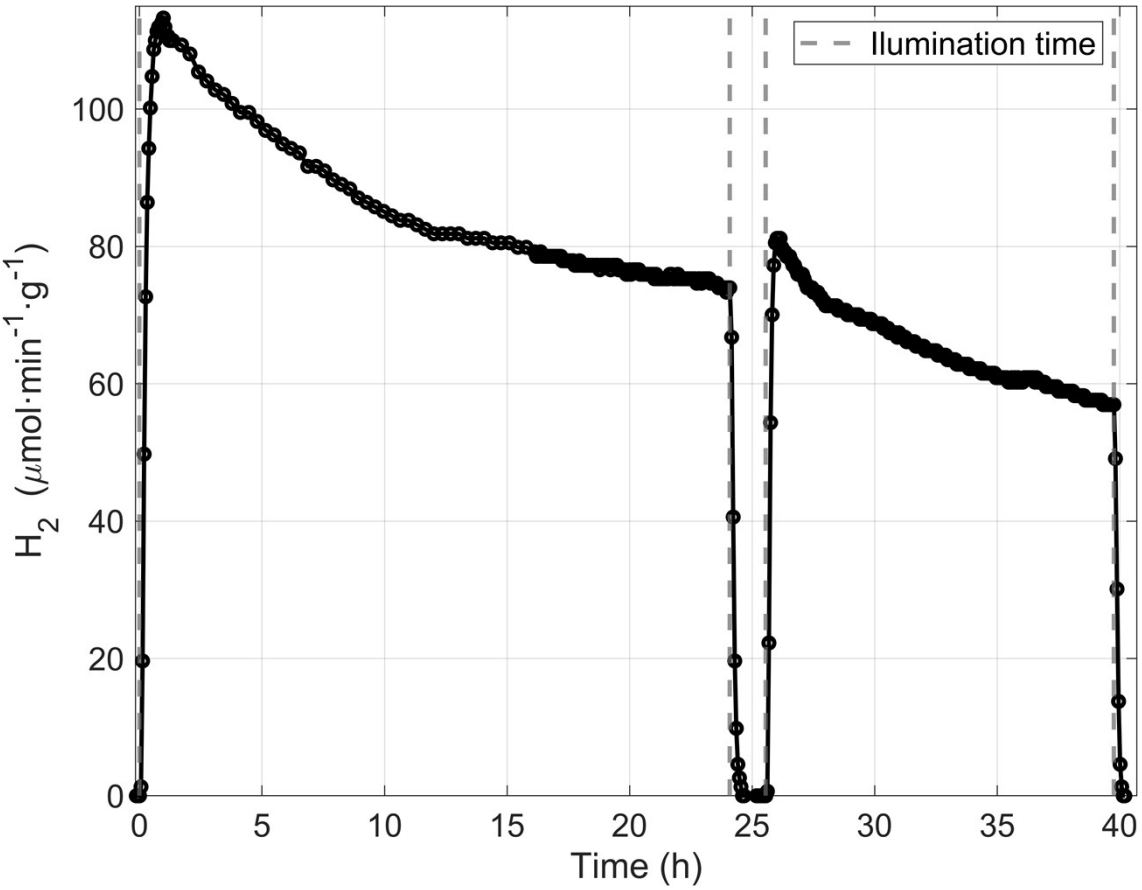

Figure S7 Extended photocatalytic stability measurements of the T-Mg4-Au sample. The sample was remeasured several months after the initial 2h photocatalytic test. Hydrogen production rate as a function of time during consecutive long-term cycles, including a 24 h continuous operation followed by a 14.5 h cycle after a resting period with air exposure. The data illustrate the gradual activity decay under continuous operation and the partial recovery of the photocatalytic performance between cycles.

Table S3 Comparison of hydrogen production rates for representative TiO_2-based photocatalytic systems reported in the literature. The table includes different catalyst configurations (planar films, nanopowders, and supported systems), reactor types (batch and continuous flow), illumination sources, and the presence of electron- (ETL) and hole-selective (HTL) components.

Stack	Photocatalyst configuration	Reactor type	Light source	ETL	HTL	Mean rate	Ref
TiO_2/Au	Planar/thin film	Continuous gas reactor	Mercury-Xenon arc lamp, 72 mW/cm^2 (UV-A)	-	Au NPs	4.0 mmol h^{-1} g^{-1}	This work
TiO_2/MgO_x/Au (most interdigitated sample, T-Mg4-Au)	Planar/thin film	Continuous gas reactor	Mercury-Xenon arc lamp, 72 mW/cm^2 (UV-A)	Mg-MgO_x (highly interdigitated)	Au NPs	8.0 mmol h^{-1} g^{-1}	This work
TiO_2/Au	Nanopatterned mesoporous film	Continuous gas reactor	LED light both UVA (365 nm, 82 mW cm^{-2}) and visible light (CCT6000K)	-	Au NPs	8.5 mmol h^{-1} g^{-1}	2
TiO_2(P90)/ AuL1NPs	Nanopowders over a cellulose support	Continuous gas reactor	LED light both UVA (365 nm, 80 mW cm^{-2}) and visible light (CCT6000K)	-	thiocoumarin-based Au(I) complexes	11.5 mmol h-1g-1	3
TiO_2/Au (101)	Nanopowders over a cellulose support	Continuous gas reactor	LED light 365 nm	-	Au NPs	5.5 mmol h^{-1} g^{-1}	4
TiO_2/Au/CNT	Nanopowders suspension in a water ethanol mixture	Continuous gas reactor	Mercury-Xenon arc lamp, 200-600 nm	CNT	Au	5.5 mmol h^{-1} g^{-1}	5
TiO_2/ZnO/Au	Nanopowders suspension in a water methanol mixture	Batch reactor	UV Lamps (254 nm) 4.4 mW/cm^2	ZnO	Au	1.9 mmol h^{-1} g^{-1}	6
TiO_2/ZnO/Au	Nanopowders suspension in a water Na_2S/Na_2SO_3 mixture	Batch reactor	Xe lamp with filters (λ > 420 nm)	ZnO	Au	0.3 mmol h^{-1} g^{-1}	7
TiO_2/SnO/Au	Nanopowders suspension in a water methanol mixture	Batch reactor	UV Lamps (254 nm) 3.6 mW/cm^2	SnO	Au	0.5 mmol h^{-1} g^{-1}	8
TiO_2/MgO/Au	Nanopowders suspension in a water	Batch reactor	W lamp 45 mW/cm^2	MgO	Au	11 mmol h^{-1} g^{-1}	9
TiO_2/CdS/Au	Nanopowders suspension in a water Na_2S/Na_2SO_3 mixture	Batch reactor	Xe lamp with filters (λ > 420 nm)	CdS	Au	3.6 mmol h^{-1} g^{-1}	10
TiO_2/ZrO/Au	Nanopowders suspension in a water methanol mixture	Batch reactor	Xenon lamp, 200-600 nm	ZrO_x	Au	4.2 mmol h^{-1} g^{-}	11

References

1 N. Chaulagain, K. M. Alam, S. Kadian, N. Kumar, J. Garcia, G. Manik and K. Shankar, Synergistic Enhancement of the Photoelectrochemical Performance of TiO2Nanorod Arrays through Embedded Plasmon and Surface Carbon Nitride Co-sensitization, *ACS Appl. Mater. Interfaces*, 2022, **14**, 24309–24320.

2 M. Torras, P. Molet, L. Soler, J. Llorca, A. Roig and A. Mihi, Au/TiO2 2D-Photonic Crystals as UV–Visible Photocatalysts for H2 Production, *Adv. Energy Mater.*, DOI:10.1002/aenm.202103733.

3 A. Agrelo-Lestón, J. Llorca, E. Martínez, I. Angurell, L. Rodríguez and L. Soler, Thiocoumarin-based Au(I) Complexes and Au(0) Systems over TiO2 as Hybrid Photocatalysts for Hydrogen Generation under UV–Vis Light, *Advanced Science*, DOI:10.1002/advs.202404969.

4 Y. Chen, L. Soler, C. Cazorla, J. Oliveras, N. G. Bastús, V. F. Puntes and J. Llorca, Facet-engineered TiO2 drives photocatalytic activity and stability of supported noble metal clusters during H2 evolution, *Nat. Commun.*, DOI:10.1038/s41467-023-41976-2.

5 J. Farah, F. Malloggi, F. Miserque, J. Kim, E. Gravel and E. Doris, Continuous Flow Photocatalytic Hydrogen Production from Water Synergistically Activated by TiO2, Gold Nanoparticles, and Carbon Nanotubes, *Nanomaterials*, DOI:10.3390/nano13071184.

6 D. Ramírez-Ortega, D. Guerrero-Araque, P. Acevedo-Peña, E. Reguera, H. A. Calderon and R. Zanella, Enhancing the photocatalytic hydrogen production of the ZnO–TiO2 heterojunction by supporting nanoscale Au islands, *Int. J. Hydrogen Energy*, 2021, **46**, 34333–34343.

7 Y. Liang, W. Li, X. Wang, R. Zhou and H. Ding, TiO2–ZnO/Au ternary heterojunction nanocomposite: Excellent antibacterial property and visible-light photocatalytic hydrogen production efficiency, *Ceram. Int.*, 2022, **48**, 2826–2832.

8 Á. Mantilla, D. Guerrero-Araque, J. H. Sierra-Uribe, L. Lartundo-Rojas, R. Gómez, H. A. Calderon, R. Zanella and D. Ramírez-Ortega, Highly efficient mobility, separation and charge transfer in black SnO2-TiO2 structures with co-catalysts: the key step for the photocatalytic hydrogen evolution, *RSC Adv.*, 2024, **14**, 26259–26271.

9 Y. Li, Y. K. Peng, L. Hu, J. Zheng, D. Prabhakaran, S. Wu, T. J. Puchtler, M. Li, K. Y. Wong, R. A. Taylor and S. C. E. Tsang, Photocatalytic water splitting by N-TiO2 on MgO (111) with exceptional quantum efficiencies at elevated temperatures, *Nat. Commun.*, DOI:10.1038/s41467-019-12385-1.

10 Y. Liang, J. Sun, Y. Lu, M. Xiu, J. Zhang, J. Yue, W. Li, H. Ding, G. Xu, C. Xue and Y. Huang, Excellent visible-light photocatalytic hydrogen production efficiency: Hollow-structured TiO2/CdS/Au or hollow-structured TiO2/Au/CdS ternary heterojunction nanocomposites?, *J. Alloys Compd.*, DOI:10.1016/j.jallcom.2024.173629.

11 L. A. Arce-Saldaña, U. Caudillo-Flores, R. Sayago-Carro, G. Soto-Herrera, M. Fernández-García and A. Kubacka, Hydrogen photoproduction using Au promoted ZrOx-TiO2 composite catalysts, *Catal. Today*, DOI:10.1016/j.cattod.2023.114148.